Biophysical Journal, Volume *120*

Supplemental information

Fluorescence intensity fluctuation analysis of receptor oligomerization in membrane domains

Gabriel Biener, Michael R. Stoneman, and Valerică Raicu

Supporting Materials

Fluorescence Intensity Fluctuation Analysis of Receptor Oligomerization in Membrane Domains

Gabriel Biener[1], Michael R. Stoneman[1], Valerică Raicu[1,2]

[1]Physics Department, University of Wisconsin – Milwaukee, Milwaukee, Wisconsin, USA
[2]Department of biological sciences, University of Wisconsin – Milwaukee, Milwaukee, Wisconsin, USA

Supplementary Note 1. - Determination of effective monomeric brightness from fluorescence images of cells expressing monomeric or dimeric fluorescence molecules

The effective monomeric brightness, ε_{eff}^{mono}, distribution was determined using de-punctate fluorescence images of Flp-In™ T-REx™ 293 cells expressing either the monomeric (PM-1-mEGFP) or a tandem-dimer (PM-2-mEGFP) of the fluorescent marker. First, regions of interest (ROIs) were drawn on the fluorescence images demarcating only the basolateral portion of the membrane, and then these ROIs were divided into square segments; the maximum area of each of the segments was 484 pixels^2. Next, we calculated the molecular brightness, ε_{eff},and concentration, C_m, values for each segment and then assembled the brightness values into a brightness distribution curve; only brightness values, corresponding to segments with concentrations between 750 and 1600 protomers × μm^{-2} were used to construct the brightness distribution. In order to calculate the fluorescent molecule concentration, we needed to input a value of ε_{eff}^{mono} (of which we were trying to determine), at this step. Therefore, in an intermediate step we used the previously published monomeric brightness of 64.8 (1) as a first guess. Finally, we fitted the brightness distribution with a sum of four Gaussians. The mean value of each of the Gaussians corresponded to the peak brightness value from a particular oligomer size (monomer, dimer, trimer, and tetramer for the PM-1-mEGFP sample and monomer, dimer, tetramer, and hexamer for PM-2-mEGFP sample) and were therefore set equal to $n\varepsilon_{eff}^{mono}$ where *n* represents the size of the oligomer. The standard deviations, σ, of all the Gaussians were set equal to each other. The fitting was accomplished by minimizing the discrepancy between the measured data and the fitting curve. The minimization was obtained by applying an iterative fitting approach which utilized the Nelder-Mead method (2, 3). The parameters which were allowed to vary during the fitting process were ε_{eff}^{mono}, σ, as well as the amplitudes of all the Gaussians.

We deconvoluted all brightness spectrograms obtained from hSecR expressing cells using three different monomeric brightness distributions. The three different monomeric brightness distributions were determined by applying the monomeric brightness determination process (described in the previous paragraph) to: (i) the fluorescence images of only the PM-1-mEGFP sample, (ii) only the PM-2-mEGFP sample, or (iii) both the PM-1-mEGFP sample and PM-2-mEGFP sample combined. The last value required simultaneous fitting of both distributions. Examples of the results from simultaneously fitting the brightness distributions of the PM-1-

mEGFP sample and PM-2-mEGFP sample are presented in supplementary Fig. S1 for the de-punctate fluorescence images.

Supplementary Note 2. - Identification and separation of puncta from regions of interest

The algorithm for identification and retention of the puncta from fluorescence images builds upon the previously published algorithm for puncta removal, with steps 1-2 and 10-18 added for improved identification of puncta as well as a modified thresholding procedure (steps 28-30) of puncta where for each punctum only the surrounding pixels are used to calculate a reference intensity.

1. Calculate Median Absolute Deviation (MAD) of the image's intensity values.
2. Smoothen the Image using Wiener filter with 1.48 x MAD as the standard deviation of the noise. The smooth image is used only to segment the ROIs in the SLIC procedure and does not affect the FIF analysis of the results.
3. Segment ROI into square segments of area l_s^2 (l_s is the length of the square side in pixels)
4. Calculate center of mass for each segment; remove segments located outside of ROI.
5. Initiate a two-dimensional array, denoted as *Label-Matrix*, using the value 0 for each array element. The elements' positions in the *Label-Matrix* array are a one-to-one mapping of the pixels' positions of the fluorescence image currently analyzed.
6. Initiate a two-dimensional array, denoted as *Distance-Matrix*, using the value of infinity for each array element. The elements' positions in the *Distance-Matrix* array are a one-to-one mapping of the pixels' positions of the fluorescence image currently analyzed.
7. **While** difference between center of mass positions in step k and step k-1 is greater than threshold, do
8. **For** each segment *i* centered at (x_i, y_i)
9. Crop a square window with area of $4l_s^2$ centered at (x_i, y_i) and assemble the intensities from each pixel into a list of intensities I
10. Calculate intensity fluctuation contrast, C, by using $C = \left(Q_{75}(I) - Q_{25}(I)\right)/Median(I)$. Q_{75} and Q_{25} are the third and first quartile values of the signal's intensity list and Median is the median value of the same list.
11. **If** $C > 1$
12. **If** $I(x_j, y_j) > I(x_i, y_i)$, where j is the index of a pixel within the signal's Intensity list.
13. Intensity weight, $m = abs\left(I - I(x_i, y_i)\right)_{Max}/(2 \cdot r)$, where r is an input ratio between climbing up and sliding down.
14. **Else** $m = abs\left(I - I(x_i, y_i)\right)_{Max}/2$
15. **End if**
16. **Else** $r = 1$
17. Repeat step 14

18. End if

19. Calculate distance between pixels enclosed within the square window area, using Eqs. 3 and 4 from (4) and *m* from steps 13 or 14.
20. **If** the distance calculated in step 19 is smaller than the distance recorded in *Distance-Matrix*(x_j, y_j),
21. Replace the distance value in the corresponding element with the new distance
22. Replace the segment index in the respective element in *Label-Matrix* with *i*
23. **End If**
24. **End For**
25. Recalculate center of mass of each segment by averaging the x and y coordinate values of all the pixels that belong to the i^{th} segment
26. **End While**
27. Calculate average intensity, $\langle I \rangle_i$, for each segment resulting from steps 1-26. The position of the pixels belonging to segment *i* can be found from the *Label-Matrix* array by extracting the positions of the elements containing the value of *i*
28. Replace each pixel within a segment with the segments average value. This Image is named Segmented Image.
29. For a given segment, find the average intensity of the surrounding segment, $\langle I_{sur} \rangle$, and calculate
    $\langle I_{sur} \rangle + \|I_{sur}\|_2$, $\langle I_{sur} \rangle$ and $\|I_{sur}\|_2$ are the average and standard deviation of I_{sur}, respectively.
30. For each segment if $\langle I \rangle_i < \langle I_{sur} \rangle + \|I_{sur}\|_2$, remove segment from segment list.
31. Repeat 1-30 for all ROIs

Supplementary Note 3. - Concatenating pixel content of multiple individual puncta into a single cluster of puncta

We created a cluster of puncta by consolidating the lists of intensity values from pixels of multiple individual puncta into a single unified list of intensity values. Intensity histograms were constructed from each cluster of puncta. The full algorithm is provided below.

1. Extract individual puncta from fluorescence images using the SLIC based procedure described in supplementary note 2.
2. For each individual punctum calculate the average intensity from the list of intensity values of the individual punctum pixels.
3. Calculate the receptor concentration of each individual punctum using the punctum's average intensity and the extracted monomeric brightness.
4. Order the puncta according to receptor concentration, calculated in step 3, from lowest to highest.
5. Combine the intensity values of pixels from five sequential puncta, starting from the lowest receptor concentration (i.e., puncta 1 to 5 as ordered in step 4), to form a cluster of puncta. Repeat for each set of five sequential puncta (i.e. puncta 6-10, 11-15, etc.)

6. Create an intensity distribution from the pixels assigned to a cluster of puncta; repeat for all clusters.
7. Fit each intensity histogram, calculated in step 6, using a single Gaussian and extract mean, and standard deviation, of the fitting curve.
8. From each set of parameters extracted from step 7 along with the camera noise information using Eqs. 6 and 7 calculate the brightness, ε_{eff}, and receptor concentration, C_m.
9. Assemble a list of brightness values and receptor concentrations.
10. Continue with the FIF spectrometry analysis on the list assembled in step 9.

Even though it seems that step 3 is redundant it is useful for comparing receptor concentration values from this step with the one calculated in step 8. We expect these values to be roughly close to each other.

Supplementary Note 4. – Comparison between punctum-by-punctum analysis and clustered puncta analysis

The intensity distributions for smaller areas are harder to fit with a Gaussian curve as we observed by comparing the quality of fit of typical intensity distribution curves obtained from clusters of puncta (supplementary Fig. S3 a, c, e) to that obtained from individual puncta (supplementary Fig. S3 b, d, f). We have quantified the differences between the quality of the fit of intensity histograms obtained from individual puncta and clusters of puncta, as follows. We first divided each intensity histogram by its maximum frequency, since the intensity histograms produced as part of the punctum-by-punctum analysis are characterized by a peak frequency value far lower than the one produced by a cluster of puncta; thus, the normalization procedure places both sets of histograms on an equal footing. Next, we fitted each normalized intensity distribution with a single Gaussian function and calculated the reduced χ^2 (χ_r^2) according to Eq. 1 (see Methods section). Finally, we assembled the χ_r^2 values from all the puncta or clusters of puncta into scatter plots, shown in supplementary Fig. S4. From supplementary Fig. S4, we notice that the scatter plot of χ_r^2 values obtained from the punctum-by-punctum analysis is broader and centered at a higher value when compared with the plot of χ_r^2 values obtained from the clustered puncta analysis; this higher center value and larger spread is an indication that the typical fitting of intensity distributions generated from individual puncta is poorer than that of clusters of puncta, and therefore provides a good reason not to use a punctum-by-punctum analysis. We calculated the spread of χ_r^2 for different bin sizes in order to avoid aliasing or any adverse effects that the choice of specific bin size has on the results. The broadening and increased y position of the scatter plot centroid for the punctum-by-punctum analysis, as compared with the clustered puncta analysis, was consistent for all the different bin sizes, as is evident in supplementary Fig. S4.

Supplementary Note 5. – Simulation of fluorescence intensities of molecules embedded in a two-dimensional lattice excited by a Lorentz-Gauss beam.

In order to study the effect of using an incorrect γ factor when calculating brightness as described in **extending the FIF method to investigate hSecR oligomerization in membrane puncta** subsection in the main body, we have considered running Monte-Carlo simulations for an ensemble of molecules embedded in a two-dimensional lattice and generating a known brightness and concentration. These molecules are excited by a simulated laser beam with a Lorentz-Gauss shape and the emission from these molecules is collected by a simulated detector. We considered two different scenarios. The first scenario assumed a two-dimensional plane containing molecules placed perpendicular to the beam propagation axis, while the second assumed a plane oriented parallel to the beam propagation axis. In both cases the intensity was collected by a detector and the simulation was repeated 500 times. The 500 simulations for each case provided data for a single image segment. We have simulated 1000 segments for each scenario. The simulation algorithm is given below.

1. Select a preset molecular brightness, $\varepsilon_{eff}^{Proto}$, and a preset average number of molecules per pixel, N.
2. Construct a 3D lattice.
3. Calculate the beam intensity at each lattice node, assuming the beam is focused at the center of the lattice box, i.e., $\mathrm{I_{LG}}(x,y,z) = \frac{\omega_0^2}{\omega_z^2} e^{\left[-2\left(\frac{x^2+y^2}{\omega_z^2}\right)\right]}$, were $\omega_z^2 = \omega_0^2\left[1+\left(\frac{z}{z_R}\right)^2\right]$, $z_R = \frac{\pi\omega_0^2}{\lambda}$, ω_0 is the beam waist, and λ is the beam wavelength.
4. **For** each Segment, i
5. **For** each pixel, j, within the segment i
6. Draw a number $\mathrm{n_{ij}}$ from a Poissonian distribution centered at N which symbolizes the number of molecules for pixel j in segment i.
7. Randomly select coordinates for each molecule, k, within the lattice limiting the molecules to a 2D plane (with a normal parallel to y or z).
8. Calculate the emission from each molecule by multiplying the beam power with the molecular brightness, e.g., $\mathrm{I_{LG}^2}(\mathrm{x_{ijk}}, \mathrm{y_{ijk}}, 0) \times \varepsilon_{\mathrm{eff}}^{\mathrm{Proto}}$.
9. Sum up the emission from the entire lattice box, i.e. $\mathrm{I_{ij}} = \sum_{\mathrm{k=1}}^{\mathrm{n}} \mathrm{I_{LG}^2}\left(\mathrm{x_{ijk}}, \mathrm{y_{ijk}}, 0\right) \times \varepsilon_{\mathrm{eff}}^{\mathrm{Proto}}$.
10. **End for**, j
11. **End for**, i

After simulating the intensities for all the pixels contained in each of the segments, we computed the brightness of a particular segment simply by using $\varepsilon_{eff}^{i} = \frac{Var(I_{ij})}{\gamma \cdot \langle I_{ij} \rangle}$. The last step was to plot the brightness histogram from all the segments. The γ factor used in the above equation can be chosen based on the assumed scenario, e.g., 0.5 for a plane perpendicular to the beam propagation axis and 0.377 for parallel to the beam propagation axis. The results from this simulation are shown in supplementary Fig. S5. Panel *a* illustrates the case where all the molecules are placed in a plane perpendicular to the beam propagation axis. Panels *b* and *c* illustrates the scenario of illuminating molecules embedded in a plane parallel to the beam propagation axis for two different γ values: using the correct γ value of 0.377 for a parallel orientation of the membrane (panel *c*), and using

the γ from the scenario corresponding to panel *a*, i.e., using an incorrect γ value of 0.5. As can be seen, the brightness histogram shifted (in supplementary Fig. S5 *b*) towards lower brightness values. This shift qualitatively agrees with the shift seen in Fig. 3, *b* and *e* and Fig. 2, *b* and *e.*

SUPPORTING REFERENCES

1. Stoneman, M. R., G. Biener, R. J. Ward, J. D. Pediani, D. Badu, A. Eis, I. Popa, G. Milligan, and V. Raicu. 2019. A general method to quantify ligand-driven oligomerization from fluorescence-based images. *Nat. Methods.* 16:493-496, doi: 10.1038/s41592-019-0408-9.
2. Ward, R. J., J. D. Pediani, S. Marsango, R. Jolly, M. R. Stoneman, G. Biener, T. M. Handel, V. Raicu, and G. Milligan. 2020. Chemokine receptor CXCR4 oligomerization is disrupted selectively by the antagonist ligand IT1t. *J. Biol. Chem.*, doi: 10.1074/jbc.RA120.016612.
3. Stoneman, M. R., N. Raicu, G. Biener, and V. Raicu. 2021. Fluorescence-based Methods for the Study of Protein-Protein Interactions Modulated by Ligand Binding. *Curr. Pharm. Des.* in press, doi.
4. Achanta, R., A. Shaji, K. Smith, A. Lucchi, P. Fua, and S. Susstrunk. 2012. SLIC Superpixels Compared to State-of-the-Art Superpixel Methods. *ITPAM.* 34:2274-2281, doi: 10.1109/Tpami.2012.120.

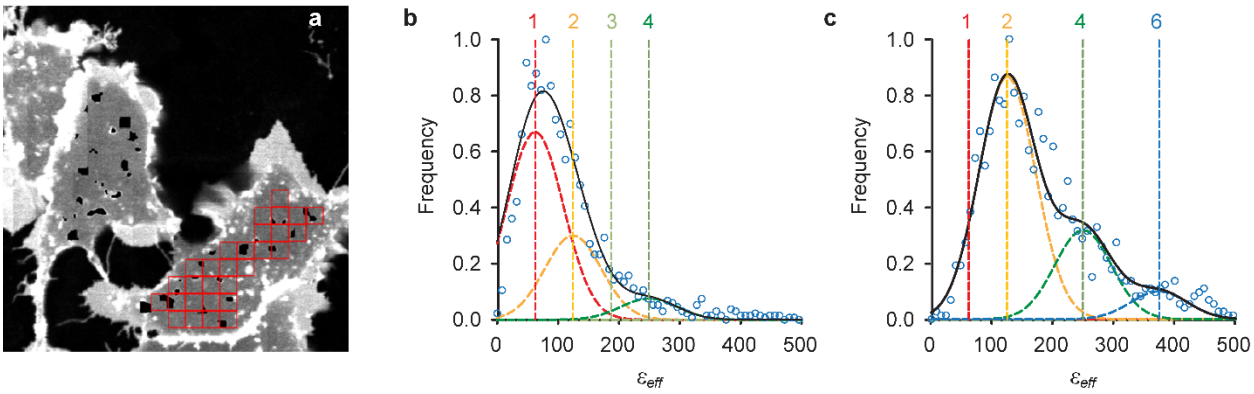

FIGURE S1 Calculation of monomeric brightness using de-punctate fluorescence images of brightness standards. De-punctate fluorescence images were obtained from cells expressing PM1-mEGFP and PM2-mEGFP anchored to the membrane**.** The calculation of the monomeric brightness was performed on these images (a-c) after puncta have been removed. (a) Example of two photon excitation scanning microscope image of basolateral membrane after puncta are removed is shown with segment boundaries superimposed (red squares). Brightness histograms assembled from de-punctate fluorescence images of cells expressing PM-1-mEGFP (b) and PM-2-mEGFP (c) were simultaneously fitted with a sum of four Gaussians. The PM1 samples were fitted with Gaussians representing monomer, dimer, trimer and tetramer (mean positions are indicated with the vertical dashed lines), The PM2 samples were fitted with Gaussians representing monomer, dimer tetramer and hexamer. The monomeric brightness found for the analysis performed on images with high intensity puncta removed was $\varepsilon_{eff}^{mono} = 62.3 \pm 46.5$.

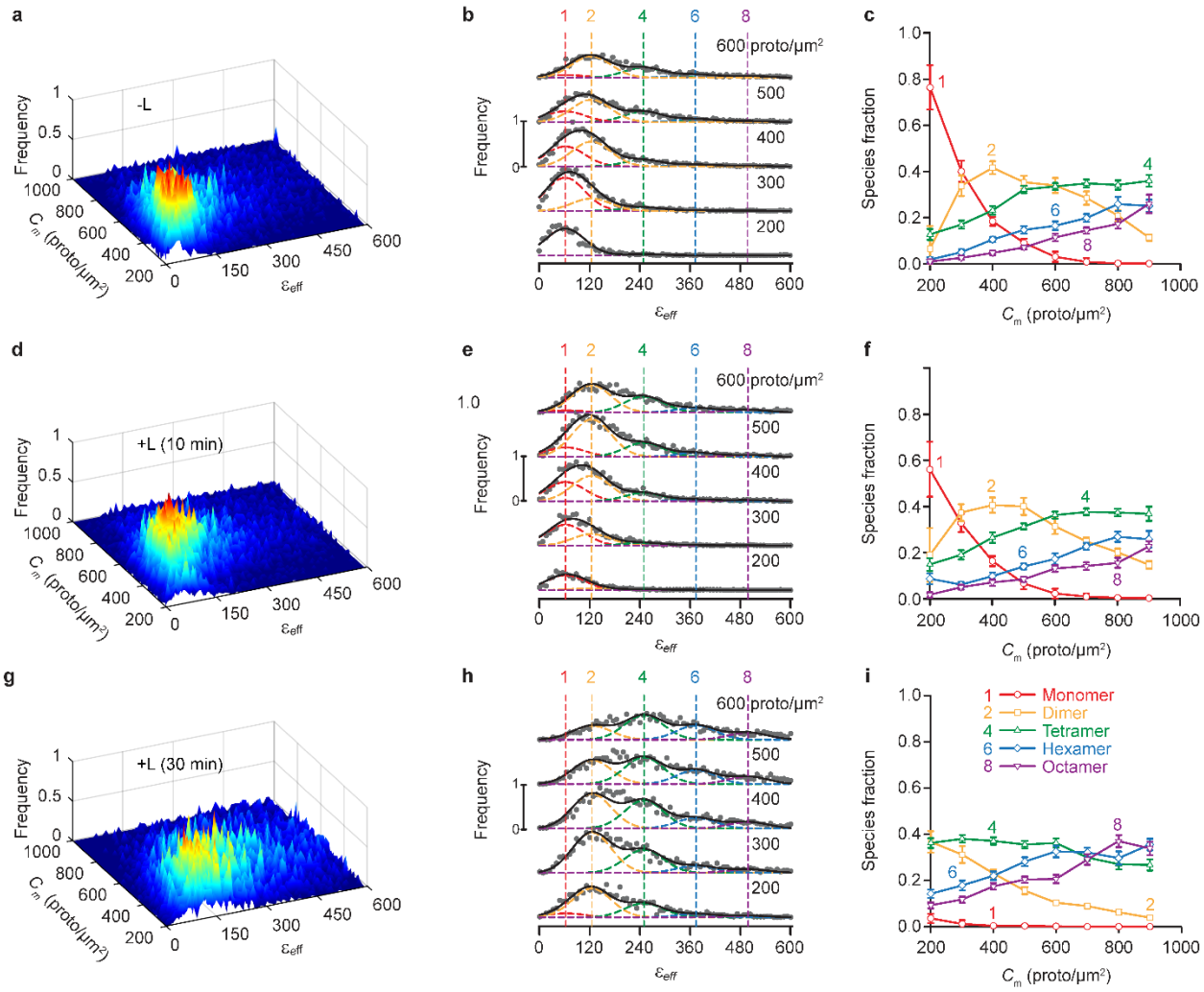

FIGURE S2 2D-FIF spectrometry applied to fluorescence images with puncta included (whole membrane analysis). Analysis was performed on the same fluorescence images which were used to obtain the results shown in Fig. 2. (a, d, g) Surface plots of the ε_{eff} occurrence frequency vs concentration of protomers using 13,393 (a), 15,288 (d) and 12,964 (g) total segments (with each segment having maximum area of 22 × 22 pixels). (b, e, h), Stacks of cross-sections through the surface plots in (a), (d), and (g), respectively, average concentration for each range (in protomers x μm^{-2}) is indicated above each curve. The vertical dashed lines indicate the peak positions for the brightness spectra of monomers ($\varepsilon_{eff}^{mono} = 62.3$), dimers and so on, obtained from the simultaneous fitting of the PM-1- and PM-2-mEGFP spectrograms used as standards of brightness (supplementary Fig. S1). (c, f, i) Relative concentration of protomers in each oligomeric species versus total concentration of protomers, as derived from fitting of the curves in (b), (e), and (h), respectively, with a sum of different Gaussian components representing different oligomeric species. Each data point and its error bar represent the mean ± s.d., respectively, of 900 different species fraction values, obtained using the bootstrapping procedure described in the Methods section.

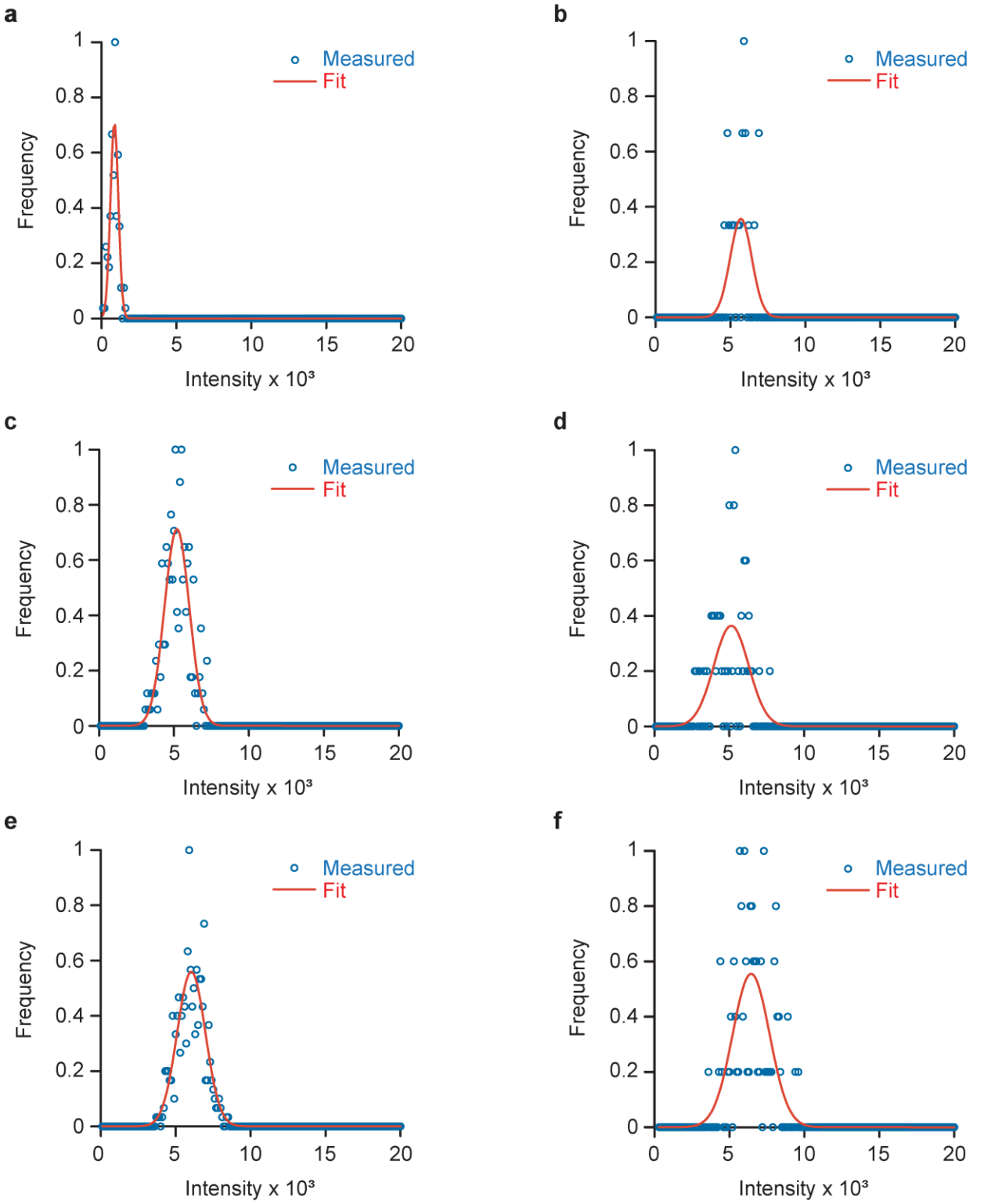

FIGURE S3 Comparison of typical intensity distributions, fitted with a single Gaussian curve, obtained from clustered puncta and individual punctum. (a-f), Measured intensity distributions (blue circles) were fitted with a single Gaussian function (red solid line) for three typical clustered puncta (a, c, e) and three typical individual punctum (b, d, f). The clustered puncta areas are 131 pixels (a), 253 pixels (c), and 392 pixels (e). The punctum areas are 19 pixels (b), 50 pixels (d), and 86 pixels (f).

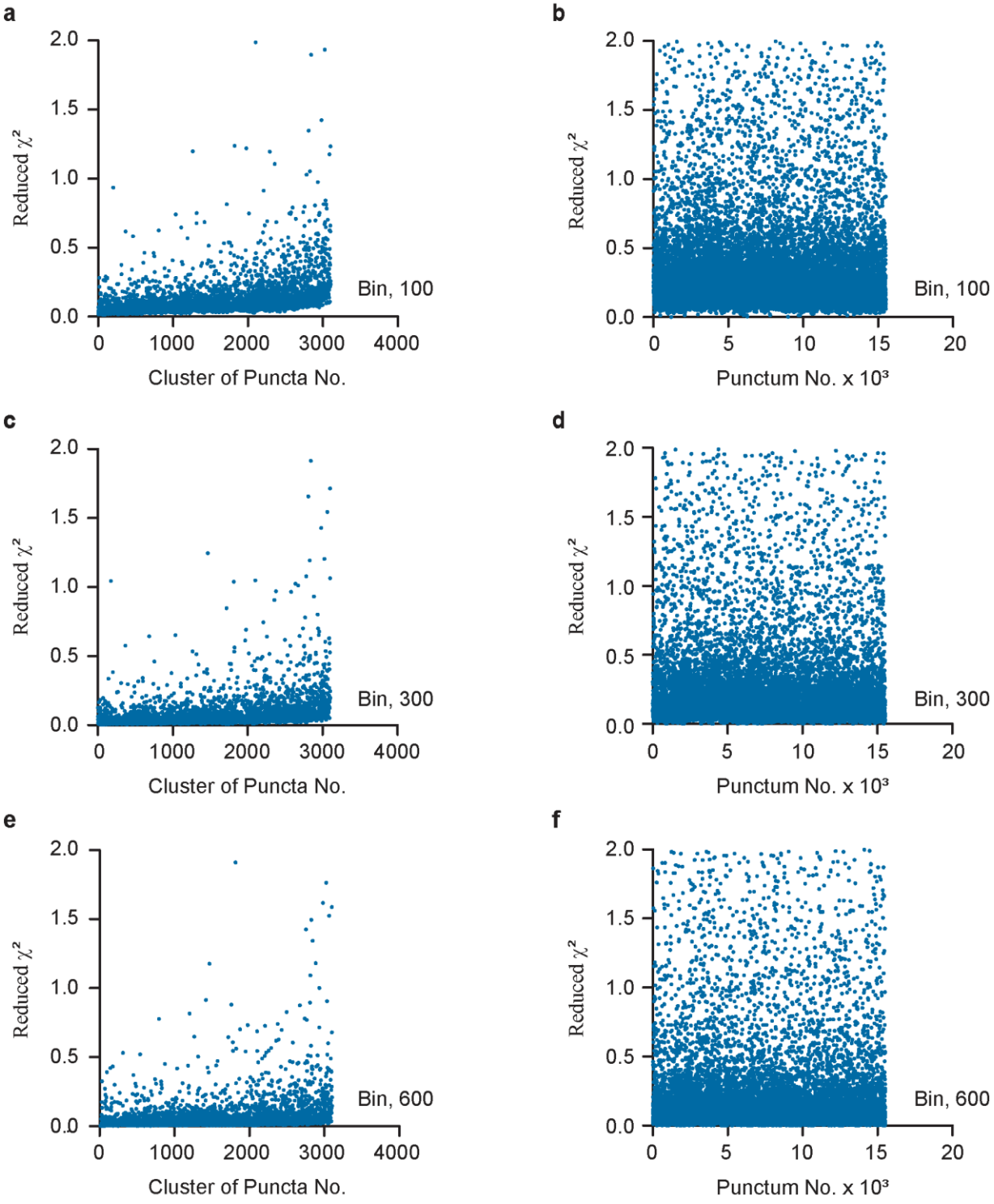

FIGURE S4 Reduced χ^2 calculated for the fitting of a single Gaussian curve to a cluster of puncta or individual punctum intensity distribution for different intensity bins. Scatter plot of reduced χ^2 versus (a, c, e) clusters of puncta number and (b, d, f) punctum number. Each point in the scatter plots represents the reduced χ^2 value obtained by fitting a Gaussin to a single intensity distribution generated from the pixel level intensities within either a cluster of puncta or a punctum. Reduced χ^2 is calculated using Eq. 1. The intensity distributions were generated using different intensity bin sizes of (a, b) 100, (c, d) 300, and (e, f) 600. The results were obtained from the untreated sample of cells expressing WT-Secretin receptors attached to mEGFP.

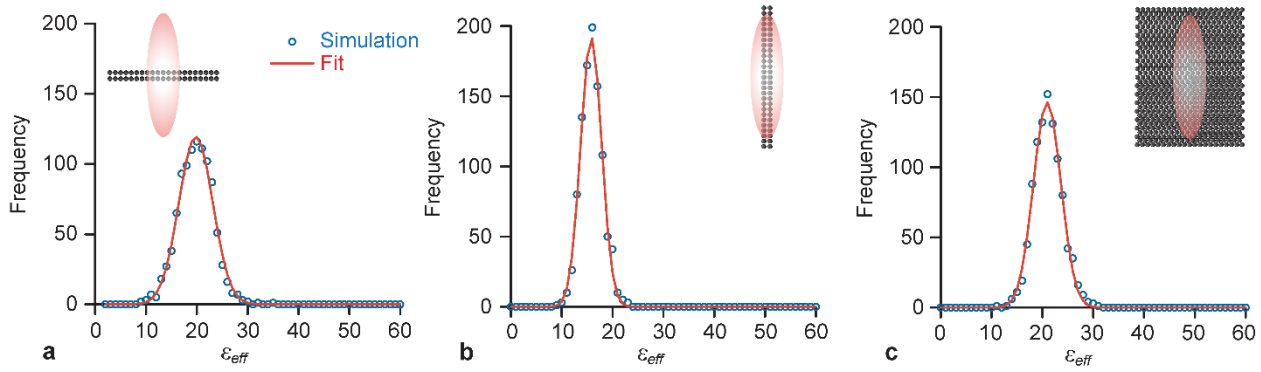

FIGURE S5 Results of the Monte-Carlo simulations of monomeric molecules placed randomly on a lattice and illuminated with a Lorentzian-Gaussian beam for different illumination and analysis scenarios. Brightness histogram of the monomeric molecules embedded in a plane perpendicular (a) or parallel (b, c) to the optical axis analyzed with the assumption of perpendicular (a, b) or parallel (c) illumination. The simulated data in (b) were therefore calculated using an incorrect γ value, which explains the shift in the brightness histogram to values lower than the brightness value of 20 used for the monomers in the simulation. Number of segments simulated was 1000 and each segment contained 500 pixels. For simplicity, the segment brightness was calculated as the $Var(I_{Seg})/\langle I_{Seg}\rangle$. Insets in a-c represent a sketch of the PSF of the laser beam (red oval shape) exciting the membrane (black rectangle) oriented perpendicular or parallel to the beam propagation axis (z axis).

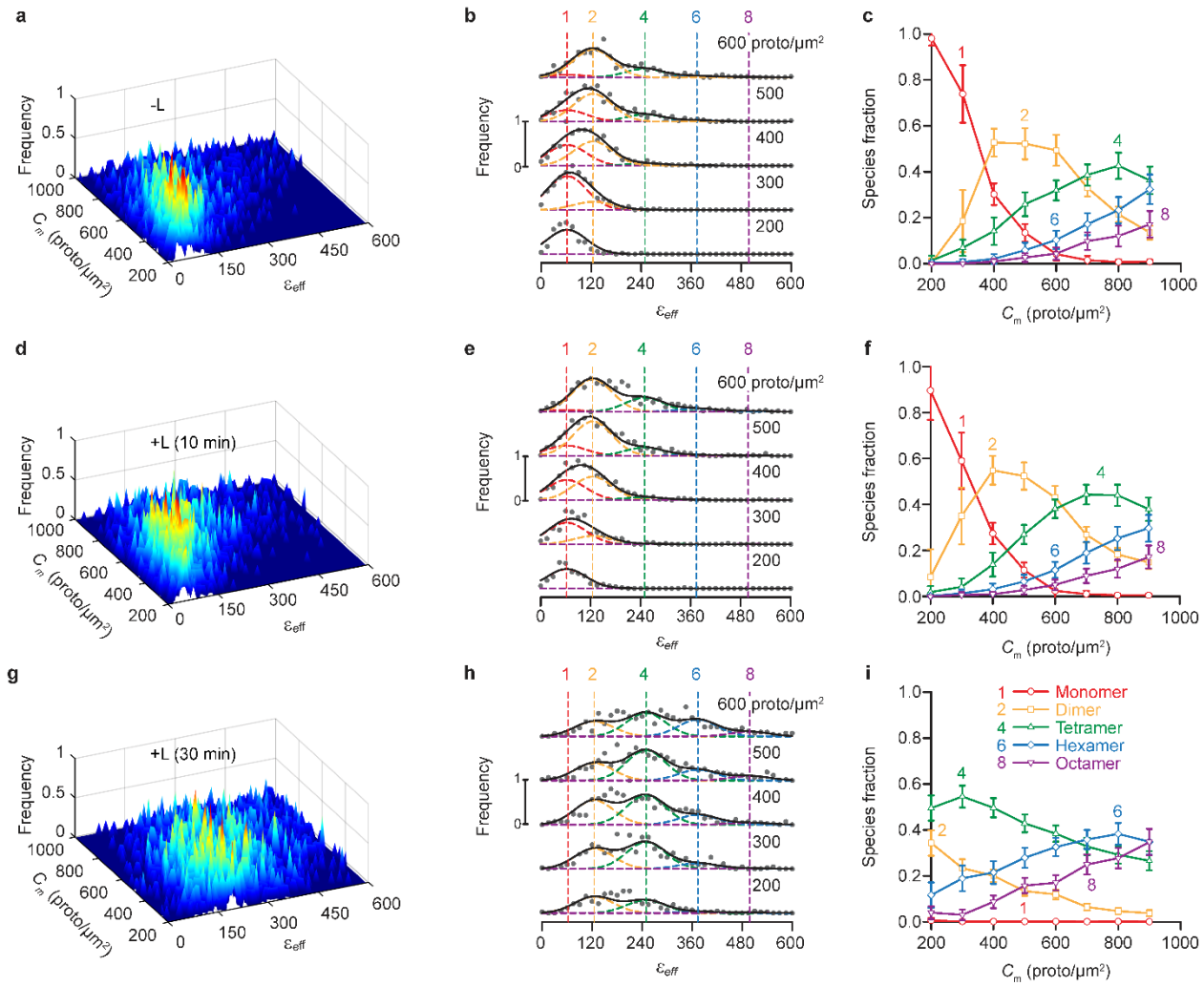

FIGURE S6 Results of the reanalysis of the data in Fig. 3 using a different γ factor as well as different PSF area factor in the calculation of *C*. The analysis was performed on the same extracted puncta from the same images as in Fig. 3. (a, d, g), Surface plots of the ε_{eff} occurrence frequency vs. receptor concentration of protomers using (a) 3,103, (d) 3,677, and (g) 3,704 total puncta clusters. (b, e, h), Stacks of cross-sections taken from the surface plots in (a), (d), and (g), respectively. Average receptor concentration for each range (in protomers x μm^{-2}) is indicated above each curve (see explanation in Fig. 2). The vertical dashed lines indicate the peak positions for the brightness spectra of monomers ($\varepsilon_{eff}^{mono} = 62.3$), dimers and so on (see Methods section). The monomeric brightness was extracted from the de-punctate areas of the monomer and tandem-dimer standard samples (c, f, i), Relative receptor concentration of protomers in each oligomeric species versus total receptor concentration of protomers, as derived from fitting of the curves in (b), (e), and (h), respectively, with a sum of different Gaussian components representing different oligomeric species. Each data point and its error bar represent the mean ± S.D., respectively, of 900 different relative fraction values, obtained from the statistical "bootstrapping" procedure mentioned in Fig. 2. γ equals 0.4423 (for Fig. 3, γ is 0.5) and the PSF area factor equals 0.173 (for Fig. 3 the PSF area factor is 0.1445).